Published in final edited form as:
Nat Struct Mol Biol. 2005 January ; 12(1): 32–37. doi:10.1038/nsmb880.

Bicarbonate activation of adenylyl cyclase via promotion of catalytic active site closure and metal recruitment

Clemens Steegborn[1], **Tatiana N Litvin**[2,3], **Lonny R Levin**[2], **Jochen Buck**[2], and **Hao Wu**[1]

[1]Department of Biochemistry, Weill Medical College of Cornell University, 1300 York Avenue, New York, New York 10021, USA

[2]Department of Pharmacology, Weill Medical College of Cornell University, 1300 York Avenue, New York, New York 10021, USA

Abstract

In an evolutionarily conserved signaling pathway, 'soluble' adenylyl cyclases (sACs) synthesize the ubiquitous second messenger cyclic adenosine 3′,5′-monophosphate (cAMP) in response to bicarbonate and calcium signals. Here, we present crystal structures of a cyanobacterial sAC enzyme in complex with ATP analogs, calcium and bicarbonate, which represent distinct catalytic states of the enzyme. The structures reveal that calcium occupies the first ion-binding site and directly mediates nucleotide binding. The single ion–occupied, nucleotide-bound state defines a novel, open adenylyl cyclase state. In contrast, bicarbonate increases the catalytic rate by inducing marked active site closure and recruiting a second, catalytic ion. The phosphates of the bound substrate analogs are rearranged, which would facilitate product formation and release. The mechanisms of calcium and bicarbonate sensing define a reaction pathway involving active site closure and metal recruitment that may be universal for class III cyclases.

The ubiquitous second messenger cAMP regulates a large variety of essential physiological processes such as gene expression, chromosome segregation and cellular metabolism. In mammalian cells, cAMP is synthesized by a family of nine transmembrane adenylyl cyclases (tmACs) and one sAC[1]. Unlike tmACs, which localize to the cellular membrane and respond to extracellular stimuli via heterotrimeric G proteins[1], sAC is found in various intracellular compartments such as the mitochondria and the nucleus[2]. Its localization near intracellular cAMP targets is the impetus for current models of second messenger signal transduction, in which cAMP functions as a locally acting signaling molecule[2–4].

sAC is insensitive to the tmAC regulators calmodulin and heterotrimeric G proteins as well as the nonphysiological activator forskolin; instead, sAC senses physiological levels of bicarbonate[5]. Aside from its role as a universal physiological buffer maintaining cellular and extracellular pH, bicarbonate functions as a signaling molecule[3], regulating many biological processes in mammals such as fertility[6], acid-base homeostasis, breathing rate, metabolism and fluid transport (reviewed in ref. 7). As the only known signaling enzyme sensitive to physiological fluctuations of bicarbonate[5], sAC probably mediates each of these processes. Bicarbonate activation of sAC is essential for sperm motility[8] as well as for pH-dependent

Correspondence should be addressed to H.W. (haowu@med.cornell.edu).
[3]Present address: Cancer Institute of New Jersey, New Brunswick, New Jersey 08901, USA.

Note: Supplementary Information is available on the Nature Structural & Molecular Biology web site.

COMPETING INTERESTS STATEMENT
The authors declare that they have no competing financial interests.

acid secretion in the epididymis and possibly the kidney[9]. In addition to its bicarbonate sensitivity, sAC is synergistically activated by calcium[10], and this potentiation seems to be important for sperm maturation[11].

Previous work has revealed the overall structure of tmAC enzymes and suggested a two-metal ion mechanism for catalysis[12,13]. Despite their different regulation, mammalian sAC and tmACs are grouped into the nucleotidyl cyclase class III based on sequence similarities within their catalytic domains[14]. We set out to study the molecular basis for the unique regulation of sAC enzymes through bicarbonate and calcium. Here, we describe a series of high-resolution crystal structures of the sAC homolog CyaC from the cyanobacterium *Spirulina platensis* in complex with ATP analogs, magnesium, calcium or calcium analogs, and with or without bicarbonate. The structures show that calcium activates sAC enzymes by replacing an active site magnesium ion that coordinates the substrate ATP. In contrast, bicarbonate stimulates sAC activity by inducing a large conformational change that leads to a remodeling of the bound nucleotide. These structures of various enzyme states further suggest general mechanisms for the catalytic pathway of class III nucleotidyl cyclases and their activation.

RESULTS

CyaC as model system for mammalian sAC enzymes

The nucleotidyl cyclase class III includes many bacterial and all known eukaryotic adenylyl and guanylyl cyclases[14]. However, the catalytic domains of mammalian sAC are more closely related to bacterial class III ACs than to any other known mammalian cyclases[15]. We therefore studied the regulation of the catalytic domain of the sAC homolog CyaC from the cyanobacterium *S. platensis* (26% sequence identity), which carries all sequence properties specific for sAC enzymes[14]. Like the mammalian enzyme[10], the catalytic domain of CyaC is stimulated by bicarbonate through an increase in its V_{max}, potentiated by calcium through an increase in the low basal affinity for the substrate ATP typical for sAC enzymes, and is synergistically activated when both compounds are present (Supplementary Fig. 1 online). Therefore, coincident bicarbonate and calcium sensing via cAMP production seems to be an ancient and conserved biological mechanism, and CyaC can serve as a model system for studying sAC activation.

α,β-Me-ATP binds to an open enzyme state

To explain the molecular basis of sAC regulation, we determined a series of structures of the CyaC catalytic domain cocrystallized with the ATP analogs α,β-methylene-adenosine-5′-triphosphate (α,β-Me-ATP; K_i = 0.3 mM) or adenosine-5′-Rp-α-thio-triphosphate (Rp-ATPαS; $K_i \approx 0.1$ mM), in the presence of magnesium as well as calcium or calcium analogs, and with or without bicarbonate, at a resolution of up to 1.9 Å (Table 1). Although sACs have unique regulatory properties, the overall structure and active site of CyaC (Fig. 1a,b) closely resemble the known structure of mammalian tmAC[12]. The only difference is that CyaC is a symmetrical homodimer of a single catalytic domain with two complete active sites, whereas tmACs are pseudo symmetrical heterodimers of structurally similar catalytic domains (C_1 and C_2), resulting in one active site and one degenerate pseudo active site.

The cocrystal structures of the cyanobacterial sAC (CyaC; from now on referred to as sAC) differed depending on which ATP analog was used. Previously, a Gαs-bound tmAC structure in the absence of nucleotide revealed a more open state than in the presence of Rp-ATPαS, suggesting that substrate binding induces closure of the active site[12,13,16]. We observed a similar closed conformation for the sAC–Rp-ATPαS complex; however, the

conformation of Rp-ATPαS was not suitable for the subsequent in-line reaction (see below), and this state therefore might not resemble the substrate-bound state. The closed enzyme conformation is similar to a tmAC–Gαs complex soaked with product analogs, and it has been speculated that it resembles a product complex and that the substrate complex adopts a different conformation[12]. Indeed, we found that in sAC in complex with α,β-Me-ATP (Fig. 1a), the ATP analog assumes a conformation in which all functional groups are arranged for the subsequent in-line reaction[17] (Fig. 1b) and therefore likely resembles the conformation of the bound substrate ATP. The α-phosphate (Pα) is in minus synclinal position and oriented so that the 3′ hydroxyl, as the subsequent attacking group, and the bond to be broken between the α-phosphorus atom and the bridging function to the β-phosphate (Pβ), are arranged in a straight line. The nucleotide conformation also primes the enzyme for catalysis by arranging Pα in eclipsed position with Pβ, which repels the pyrophosphate to facilitate its release.

In contrast to the sAC–Rp-ATPαS complex, the state of the active site of the sAC–α,β-Me-ATP complex is even more open than in the tmAC–$G\alpha_s$ structure without nucleotide, manifested in a 3–4 Å outward shift of helix α1 (Fig. 1c). Modeling an ATP complex based on the sAC–α,β-Me-ATP structure revealed that ATP could adopt a conformation similar to the analog, which fits well into the open enzyme state (Supplementary Fig. 2 online). Therefore, we conclude that nucleotide binding to sAC does not necessitate active site closure; in fact, it seems to precipitate an open state poised for catalysis. The open substrate analog complex observed here for sAC might also apply to tmACs and would explain why soaking or cocrystallization of activated ($G\alpha_s$-bound) tmAC with α,β-Me-ATP was not successful[12]: in contrast to the basally active sAC enzyme used here, binding of the activator $G\alpha_s$ to tmAC may have induced partial active site closure in the absence of an ATP analog.

Calcium replaces an active site magnesium

The open state has only a single bound metal ion, rather than the two metal ions required for catalysis[16]. This ion (positioned analogously to the ion B magnesium in tmAC structures) serves as an anchoring point for ATP by coordinating and stabilizing the Pβ and γ-phosphate (Pγ) of the ATP analog. Soaking with $SrCl_2$ or $EuCl_3$, which are both known to occupy calcium sites[18,19], unambiguously identified this ion B site as a calcium-binding pocket (Fig. 1b). We found no allosteric binding sites for calcium, and soaking in the calcium analogs did not lead to any substantial conformational changes. Although calcium is not often found in active sites, the ion B site is a typical calcium-binding site formed by less flexible ligands and few solvent molecules[19,20]. The main chain carbonyl oxygen of Ile1018, the side chains of Asp1017 and Asp1061, the phosphate oxygen atoms of Pβ and Pγ of the substrate analog, and a single water molecule coordinate the ion B site calcium (Fig. 1d). The bidentate interaction with Asp1017, which results in a seven-fold coordination that is more favorable for calcium than for magnesium, probably explains the higher affinity of calcium for this site. As calcium has also been reported to have a higher affinity for ATP in solution[21], this dual preference explains how calcium lowers the K_m for ATP in both mammalian and bacterial sACs, an effect necessary for high sAC activity at physiological ATP concentrations[10] because of the enzyme's low basal substrate affinity (K_m = 12.3 mM; Supplementary Fig. 1 online).

Bicarbonate induces active site closure

Unlike calcium's ability to increase substrate affinity, bicarbonate stimulates substrate turnover. Cocrystallization of sAC with bicarbonate did not produce any crystals and soaking bicarbonate into preformed crystals dissolved them, suggesting that bicarbonate caused a structural change. Like sAC activation in solution[5] (Supplementary Table 1 online), the bicarbonate effect on sAC crystals is specific and pH-independent and cannot be

induced with other anions, such as nitrate or acetate (see Supplementary Fig. 3 and Supplementary Table 1 online). Flash soaking and freezing permitted us to catch a glimpse of the bicarbonate-induced conformational changes. Most markedly, bicarbonate induced closure of the active site and facilitated binding of the second metal ion (ion A), which serves as the catalytic metal (Fig. 2a,b and Supplementary Video 1 online).

Bicarbonate 'closes' the active site mainly by inducing a 4–5 Å movement of the β7–β8 loop toward the dimer center and a shift of the α1 helix in the same direction. This conformation is stabilized by a newly formed salt bridge between Arg1023 within the α1 helix and Asp1187* (asterisk indicates the partner monomer within the dimer) in the β7–β8 loop. The active site closure induced movements of a several active site residues conserved in all class III cyclases. The β7–β8 loop movement shifts Lys1184*, which in turn pushes Arg1150* of the neighboring α4 helix by 6 Å. Arg1150* is positioned by Asn1146* to be oriented toward the ATP ribose 3′ hydroxyl group and Pα such that it could stabilize the additional negative charge in the transition state[22]. The shift of the α1 helix rearranges the phosphate chain of the ATP analog, leading to a 180° flip of Pγ (Fig. 2c). The shift pushes Pγ out of its binding site and orients it toward Arg1117. This residue was previously thought to bind the substrate[12] but now seems to attract the reaction product pyrophosphate to aid its exit. These same structural elements were found to be flexible in the $G\alpha_s$-bound tmAC structures; therefore, we predict that $G\alpha_s$ facilitates similar conformational changes in tmACs as bicarbonate induces in sAC.

Rp-ATPαS binds nonproductively to sAC

As stated above, Rp-ATPαS binds in a nonproductive conformation to a more closed sAC state than α,β-Me-ATP (Fig. 3b). This intermediately closed enzyme state resembles $G\alpha_s$-bound tmAC soaked with Rp-ATPαS[16] and is slightly less closed than the bicarbonate-soaked sAC–α,β-Me-ATP structure. The sAC–Rp-ATPαS complex has two magnesium ions bound, and the electron density clearly reveals that instead of the pro-R oxygen being positioned for coordination of ion A, as observed in the α,β-Me-ATP structure (Fig. 1b,d) and as necessary for productive ATP binding, its replacement by sulfur in Rp-ATPαS forces Pα to turn such that the pro-S oxygen now coordinates ion A (Fig. 3c and Supplementary Fig. 4 online). This twisted conformation prevents the in-line arrangement of attacking and leaving group, that is, the ribose 3′ hydroxyl group and the bridging oxygen between the α- and β-phosphorus atoms. This observation rationalizes why Rp-ATPαS stereospecifically inhibits class III ACs[17], whereas Sp-ATPαS, whose modification does not prevent binding in a productive, α,β-Me-ATP-like conformation, is a substrate for tmACs[17] and likely for sAC enzymes (Supplementary Fig. 5 online).

The sAC–Rp-ATPαS complex, in addition to being partially closed, has the second metal ion, essential for catalytic activity, bound to the ion A site. During catalysis this ion is recruited after binding of the substrate[23], and this partially closed enzyme state with two bound ions therefore might resemble some features of an intermediate conformation of the enzyme during catalysis. This conclusion is consistent with the successful soaking of Rp-ATPαS into tmAC crystals already partially closed by $G\alpha_s$[16]. Because of its artificial binding conformation, Rp-ATPαS induced a partially closed state of sAC in the absence of bicarbonate stimulation, and soaking bicarbonate into these crystals resulted in further closure into a structure similar to the bicarbonate-soaked structure of sAC in complex with α,β-Me-ATP (Fig. 3b).

Potential bicarbonate recognition sites

Bicarbonate induced these structural changes, but it was not detected in any of the soaked crystals. Its absence, along with the observations that bicarbonate (i) does not disrupt

microcrystals of free sAC, and (ii) is very specific (Supplementary Table 1 online), yet requires high concentrations (physiological concentrations between 5 and 25 mM) to activate sAC[5,10,24] (corresponding to an estimated off-rate of ~10^6 s^{-1}, much higher than the turnover rate k_{cat} of ~1 to 4 s^{-1}; Supplementary Methods online), might suggest that bicarbonate interacts only very transiently with the enzyme during each catalytic cycle.

In the absence of a defined bicarbonate-binding site, sequence differences between tmACs and sACs provide the best insight into the unique bicarbonate regulation of sAC enzymes (Fig. 3a). One difference corresponds to sAC active site residue Thr1139*, which is conserved in the bicarbonate-responsive sACs but replaced by a conserved aspartate in bicarbonate-insensitive bacterial ACs and tmACs[24]. Mutating the analogous threonine to aspartate abolished bicarbonate responsiveness in CyaB1, a cyanobacterial sAC[24], consistent with Thr1139* contributing to the bicarbonate stimulation of sACs. A potential scenario is that a single bicarbonate molecule could replace the two water molecules that coordinate ion A (Fig. 3c) and facilitate recruitment of this catalytic ion. TmACs with an aspartate replacing sAC Thr1139* would be insensitive to bicarbonate because of the negative charge that decreases the bicarbonate population near the ion A site. However, the effect of bicarbonate on the sAC–Rp-ATPαS complex indicates that ion recruitment can be only part of the bicarbonate function.

A second sequence variation between sACs and tmACs localizes to the β4–β5 loop[14], in which bicarbonate-responsive sACs contain a single-residue insertion (Fig. 3b). The additional residue causes a different conformation of the β4–β5 strands, opening a hole in the back of the enzyme, which may be a conduit for bicarbonate access to the active site. However, we could not confirm the role of this insertion because shortening this loop by one amino acid abolished enzyme activity (data not shown).

DISCUSSION

The structures described here reveal two novel mechanisms of stimulating production of the ubiquitous second messenger cAMP by sAC enzymes. In contrast to its more common role as an allosteric regulator, calcium binds to the active site and directly contributes to substrate binding. We also show that bicarbonate, which was previously only known to serve as a substrate for enzymes, plays an allosteric role by inducing a stimulatory conformational change.

For a model for the dynamic catalytic pathway and the specific activation of all class III adenylyl and guanylyl cyclases (Fig. 4 and Supplementary Video 2 online), we assembled the structures presented here. In this model, substrate binding would lead to the formation of an enzyme–substrate complex in the open conformation, with one magnesium bound at the ion B site. In sAC enzymes, this ion can be replaced by calcium to increase substrate affinity. The next step of catalysis is binding of the second metal to the ion A site and the concomitant active site closure. This is the step facilitated by the physiological stimulators of ACs, either bicarbonate in the case of sAC enzymes or $G\alpha_s$ proteins for tmACs. Binding of the ion A magnesium enables transition state formation by contributing to the activation of the ribose 3′ hydroxyl group and by stabilizing the charges at the triphosphate. The force from the active site closure would shift Pγ and Pβ toward the front, where the products will ultimately exit. Unlike the phosphate flip observed for the α,β-Me-ATP substrate analog, Pγ and Pβ of ATP would move as a rigid body, thereby lengthening and weakening the bond to Pα (Fig. 4). The movement of Pγ and Pβ would force Pα to swing toward the 3′ hydroxyl, leading to ring formation and release of pyrophosphate. The closed conformation observed for the tmAC–$G\alpha_s$–Rp-ATPαS complex and for the sAC complexes after bicarbonate addition probably corresponds to this product complex with one major

exception: the positions of Pγ and Pβ are swapped compared with the product pyrophosphate (Fig. 4). This model is reinforced by the observation that both protein conformation and the position of pyrophosphate in a tmAC–$G\alpha_s$–product analog structure[12] match those observed in the Rp-ATPαS and bicarbonate-soaked structures. Dissociation of pyrophosphate finally enables the active site to open again by releasing the interactions of the phosphates with the α1 helix and β7–β8 loop.

In summary, the high-resolution structures of different enzyme states presented here predict that class III cyclases might use the same reaction pathway, and that modulators, such as G proteins in tmACs and bicarbonate in sAC, might increase activity by promoting the catalytic cycle via active site closure and metal recruitment.

METHODS

Cloning, protein purification and activity assays

Residues 998–1202 and 1005–1202, respectively, which comprise the catalytic domain of CyaC from *S. platensis* (TrEMBL entry O32393)[25], were cloned into the pET28a expression vector with an N-terminal His-tag and expressed in *Escherichia coli* BL21(DE3) for 18 h at 20 °C. The protein was purified using Ni-NTA affinity and Q-Sepharose ion exchange chromatography, followed by gel filtration in 20 mM Tris, pH 7.8. Adenylyl cyclase assays were carried out with purified CyaC(998–1202) as described[10]. Protein used for activity assays was stored at −20 °C in 50% (v/v) glycerol.

Crystallization and X-ray data collection

For crystallization of CyaC(998–1202) in complex with Rp-ATPαS, drops were mixed from 1 μl protein solution (8 mg ml^{-1} in 20 mM Tris, pH 7.8, 5 mM Rp-ATPαS, 7.5 mM $MgCl_2$, 10 mM $CaCl_2$) and 1 μl reservoir solution, equilibrated against 0.4 ml reservoir (100 mM HEPES, pH 7.2, 8% (w/v) isopropanol, 10% (w/v) PEG 4000), and microseeded after 24 h. CyaC(1005–1202) in complex with α,β-Me-ATP was crystallized by mixing 1 μl protein solution (6 mg ml^{-1} in 20 mM Tris, pH 7.8, 5 mM α,β-Me-ATP, 5 mM $MgCl_2$, 5 mM $CaCl_2$) and 1 μl reservoir solution and equilibration against 0.4 ml reservoir (100 mM cacodylate, pH 6.7, 6% (w/v) isopropanol, 11% (w/v) PEG 4000). Both crystal forms were frozen 60 s after addition of two-drop volumes cryoprotectant solution (25% (v/v) isopropanol in reservoir solution).

For identifying the calcium-binding site, CyaC(1005–1202)–α,β-Me-ATP crystals were soaked with 5 mM $EuCl_3$ for 23 h and with 10 mM $SrCl_2$ for 13 h, respectively. Bicarbonate soaking was done by adding 150 mM potassium bicarbonate, pH 7.5, to the cryoprotectant solution and freezing of the crystals after 15 to 25 s. Diffraction data were collected at 100 K at Brookhaven National Laboratory beamline X4A (Table 1) and indexed, scaled and merged with DENZO and SCALEPACK[26].

Structure determination

Initial Patterson search trials with the CyaC–Rp-ATPαS data and with a polyalanine model of tmAC VC_1 (PDB entry 1AZS; 20% identity with CyaC) or with conserved side chains included did not yield a prominent solution. We therefore generated a homology model of CyaC from the tmAC VC_1 structure (HM-CyaC). Only after converting HM-CyaC to a polyalanine model were we able to obtain two of the three monomers in the asymmetric unit using MOLREP[27]: monomer A, which forms a dimer with its symmetry mate along a crystallographic two-fold rotation axis and an isolated monomer B. The missing monomer C expected from Matthews coefficient calculation, crystal packing analysis and the tmAC structure was generated manually by applying two-fold rotation symmetry on B resulting in

a BC dimer. A fine grid search for C using Como[28] then located the correct orientation and position of this monomer. For rigid body refinement and simulated annealing, all monomers had to be replaced with a tmAC VC_1 model trimmed to include only the conserved core of the protein. Electron density quality was sufficient for model building after being markedly improved through three-fold noncrystallographic symmetry averaging and solvent flattening with DM[29]. Model building was done using O[30], and the model was refined using CNS[31] with an overall anisotropic *B*-factor, a bulk solvent correction and individual isotropic Debye-Waller factors. All further complex structures were solved by molecular replacement using MOLREP[27]. Structural figures were generated with MolScript[32] and Raster3D[33] (Figs. 1a,c, 2a and 3a), SETOR[34] (Figs. 1b, 2b,c and 3b), and PyMOL (http://www.pymol.org) (Fig. 1d), and the alignment (Fig. 3c) with Alscript[35].

Coordinates

The coordinates and structure factors have been deposited in the Protein Data Bank (accession codes: CyaC in complex with Rp-ATPαS, 1WC1; with α,β-Me-ATP, 1WC0, with α,β-Me-ATP and Sr^{2+}, 1WC3; with α,β-Me-ATP and Eu^{3+}, 1WC4; activated α,β-Me-ATP and Rp-ATPαS complexes after soaking with bicarbonate, 1WC5 and 1WC6, respectively).

Supplementary Material

Refer to Web version on PubMed Central for supplementary material.

Acknowledgments

We thank K. Hess and N. Stephanou for technical assistance and R. Abramowitz and X. Yang for support at National Synchrotron Light Source beamline X4A. C.S. acknowledges support as Berger Fellow of the Damon-Runyon Cancer Research Foundation, and H.W. is a Pew Scholar of Biomedical Sciences and a Rita Allen Scholar. This work was supported by funds from the US National Institutes of Health (L.R.L. and J.B.), Hirschl Weill-Caulier Trust (L.R.L.) and the Ellison Medical Foundation (J.B.).

References

1. Hanoune J, Defer N. Regulation and role of adenylyl cyclase isoforms. Annu. Rev. Pharmacol. Toxicol. 2001; 41:145–174. [PubMed: 11264454]
2. Zippin JH, et al. Compartmentalization of bicarbonate-sensitive adenylyl cyclase in distinct signaling microdomains. FASEB J. 2003; 17:82–84. [PubMed: 12475901]
3. Zippin JH, et al. Bicarbonate-responsive “soluble” adenylyl cyclase defines a nuclear cAMP microdomain. J. Cell Biol. 2004; 164:527–534. [PubMed: 14769862]
4. Bundey RA, Insel PA. Discrete intracellular signaling domains of soluble adenylyl cyclase: camps of cAMP? Sci. STKE. 2004; 2004:PE19. [PubMed: 15126677]
5. Chen Y, et al. Soluble adenylyl cyclase as an evolutionarily conserved bicarbonate sensor. Science. 2000; 289:625–628. [PubMed: 10915626]
6. Visconti PE, et al. Novel signaling pathways involved in sperm acquisition of fertilizing capacity. J. Reprod. Immunol. 2002; 53:133–150. [PubMed: 11730911]
7. Zippin JH, Levin LR, Buck J. CO(2)/HCO(3)(−)-responsive soluble adenylyl cyclase as a putative metabolic sensor. Trends Endocrinol. Metab. 2001; 12:366–370. [PubMed: 11551811]
8. Esposito G, et al. Mice deficient for soluble adenylyl cyclase are infertile because of a severe sperm-motility defect. Proc. Natl. Acad. Sci. USA. 2004; 101:2993–2998. [PubMed: 14976244]
9. Pastor-Soler N, et al. Bicarbonate regulated adenylyl cyclase (sAC) is a sensor that regulates pH-dependent V-ATPase recycling. J. Biol. Chem. 2003; 278:49523–49529. [PubMed: 14512417]
10. Litvin TN, Kamenetsky M, Zarifyan A, Buck J, Levin LR. Kinetic properties of “soluble” adenylyl cyclase. Synergism between calcium and bicarbonate. J. Biol. Chem. 2003; 278:15922–15926. [PubMed: 12609998]

11. Jaiswal BS, Conti M. Calcium regulation of the soluble adenylyl cyclase expressed in mammalian spermatozoa. Proc. Natl. Acad. Sci. USA. 2003; 100:10676–10681. [PubMed: 12958208]
12. Tesmer JJ, Sunahara RK, Gilman AG, Sprang SR. Crystal structure of the catalytic domains of adenylyl cyclase in a complex with $G\alpha_s$.GTPγS. Science. 1997; 278:1907–1916. [PubMed: 9417641]
13. Tesmer JJ, Sprang SR. The structure, catalytic mechanism and regulation of adenylyl cyclase. Curr. Opin. Struct. Biol. 1998; 8:713–719. [PubMed: 9914249]
14. Linder JU, Schultz JE. The class III adenylyl cyclases: multi-purpose signalling modules. Cell Signal. 2003; 15:1081–1089. [PubMed: 14575863]
15. Buck J, Sinclair ML, Schapal L, Cann MJ, Levin LR. Cytosolic adenylyl cyclase defines a unique signaling molecule in mammals. Proc. Natl. Acad. Sci. USA. 1999; 96:79–84. [PubMed: 9874775]
16. Tesmer JJ, et al. Two-metal-Ion catalysis in adenylyl cyclase. Science. 1999; 285:756–760. [PubMed: 10427002]
17. Eckstein F, Romaniuk PJ, Heideman W, Storm DR. Stereochemistry of the mammalian adenylate cyclase reaction. J. Biol. Chem. 1981; 256:9118–9120. [PubMed: 7263702]
18. Fox BA, et al. Identification of the calcium binding site and a novel ytterbium site in blood coagulation factor XIII by X-ray crystallography. J. Biol. Chem. 1999; 274:4917–4923. [PubMed: 9988734]
19. Pidcock E, Moore GR. Structural characteristics of protein binding sites for calcium and lanthanide ions. J. Biol. Inorg. Chem. 2001; 6:479–489. [PubMed: 11472012]
20. Katz AK, Glusker JP, Beebe SA, Bock CW. Calcium ion coordination: A comparison with that of beryllium, magnesium, and zinc. J. Am. Chem. Soc. 1996; 118:5752–5763.
21. Mohan MS, Rechnitz GA. Ion-electrode study of the calcium-adenosine triphosphate system. J. Am. Chem. Soc. 1972; 94:1714–1716. [PubMed: 5015673]
22. Yan S-Z, Huang Z-H, Shaw RS, Tang W-J. The conserved asparagine and arginine are essential for catalysis of mammalian adenylyl cyclase. J. Biol. Chem. 1997; 272:12342–12349. [PubMed: 9139678]
23. Garbers DL, Johnson RA. Metal and metal-ATP interactions with brain and cardiac adenylate cyclase. J. Biol. Chem. 1975; 250:8449–8456. [PubMed: 1194261]
24. Cann MJ, Hammer A, Zhou J, Kanacher T. A defined subset of adenylyl cyclases is regulated by bicarbonate ion. J. Biol. Chem. 2003; 278:35033–35038. [PubMed: 12829712]
25. Kasahara M, Yashiro K, Sakamoto T, Ohmori M. The *Spirulina platensis* adenylate cyclase gene, *cyaC*, encodes a novel signal transduction protein. Plant Cell Physiol. 1997; 38:828–836. [PubMed: 9297847]
26. Otwinowski Z, Minor W. Processing of X-ray diffraction data collected in oscillation mode. Methods Enzymol. 1997; 276:307–326.
27. Vagin A, Teplyakov A. MOLREP: an automated program for molecular replacement. J. Appl. Crystallogr. 1997; 30:1022–1025.
28. Jogl G, Tao X, Xu Y, Tong L. COMO: a program for combined molecular replacement. Acta Crystallogr. D. 2001; 57:1127–1134. [PubMed: 11468396]
29. Collaborative Computational Project, Number 4. The CCP4 suite: programs for protein crystallography. Acta Crystallogr. D. 1994; 50:760–763. [PubMed: 15299374]
30. Jones TA, Zou JY, Cowan SW, Kjeldgaard M. Improved methods for building protein models in electron density maps and the location of errors in these models. Acta Crystallogr. A. 1991; 47:110–119. [PubMed: 2025413]
31. Brünger AT, et al. Crystallography & NMR system: A new software suite for macromolecular structure determination. Acta Crystallogr. Sect. D. 1998; 54:905–921. [PubMed: 9757107]
32. Kraulis PJ. MOLSCRIPT: a program to produce both detailed and schematic plots of protein strucrures. J. Appl. Crystallogr. 1991; 24:946–950.
33. Merrit EA, Murphy MEP. RASTER3D Version 2.0. A program for photorealistic molecular graphics. Acta Crystallogr. Sect. D. 1994; 50:869–873. [PubMed: 15299354]
34. Evans SV. SETOR: hardware lighted three-dimensional solid model representations of macromolecules. J. Mol. Graphics. 1993; 11:134–138.

35. Barton GJ. ALSCRIPT a tool to format multiple sequence alignments. Prot. Engineering. 1993; 6:37–40.

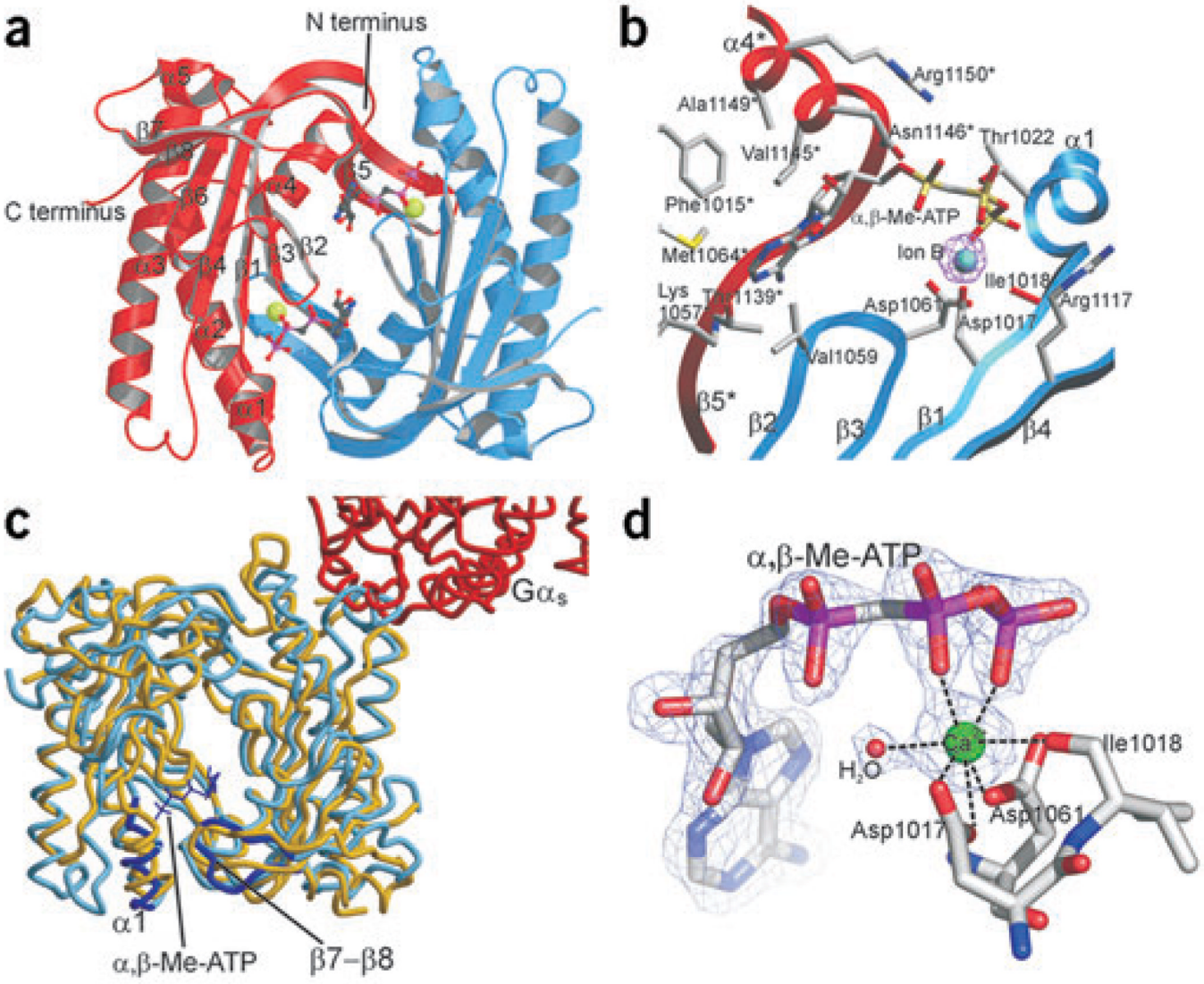

Figure 1.

Open conformation of sAC in complex with α,β-Me-ATP and calcium. (**a**) Ribbon diagram of the sAC homodimer with the substrate analog α,β-Me-ATP and one metal ion bound to each active site. The two monomers are red and blue, respectively. (**b**) Active site of the sAC–α,β-Me-ATP complex with the two monomers colored red and blue, respectively. Positive $F_o - F_c$ omit electron density after soaking with the calcium analog europium is overlaid (contoured at 8 σ), showing the single heavy atom bound at the ion B site. (**c**) Overlay of sAC–α,β-Me-ATP (blue) with the structure of $G\alpha_s$-bound tmAC (yellow and red) without substrate analog. sAC helix α1 is shifted to a more open position to avoid clashes with the substrate analog. (**d**) Close-up view of the calcium-binding pocket in the high-resolution structure of the Sr^{2+}-soaked sAC–α,β-Me-ATP complex showing the seven-fold coordination to the metal. The $2F_o - F_c$ omit electron density defining the ligands was contoured at 1.3 σ.

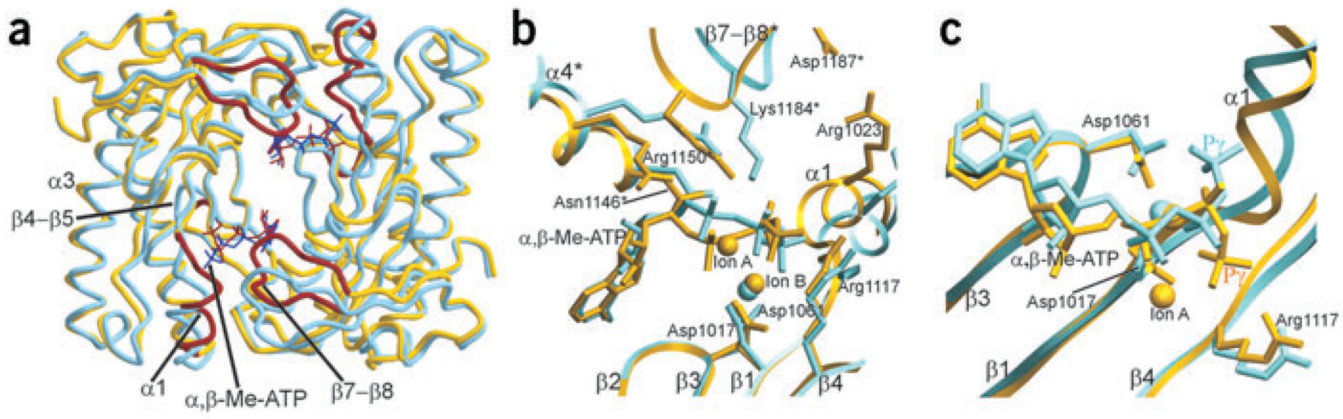

Figure 2.

Bicarbonate induces active site closure. (**a**) Overlay of sAC structures in the open state (blue) and after bicarbonate addition (yellow and red). Major conformational changes include shifts of the α1 helix and the β7–β8 strands, a flip of the loop between β4 and β5 and a kinking of helix α3 (best seen in Supplementary Video 1 online). (**b**) Active site before (blue) and after (yellow) the bicarbonate-induced active site closure, showing the recruited second metal ion and the structural rearrangements described in the text. (**c**) Close-up view for the remodeling of Pβ and Pγ of the ATP analog upon bicarbonate-induced active site closure (blue before and yellow after bicarbonate addition).

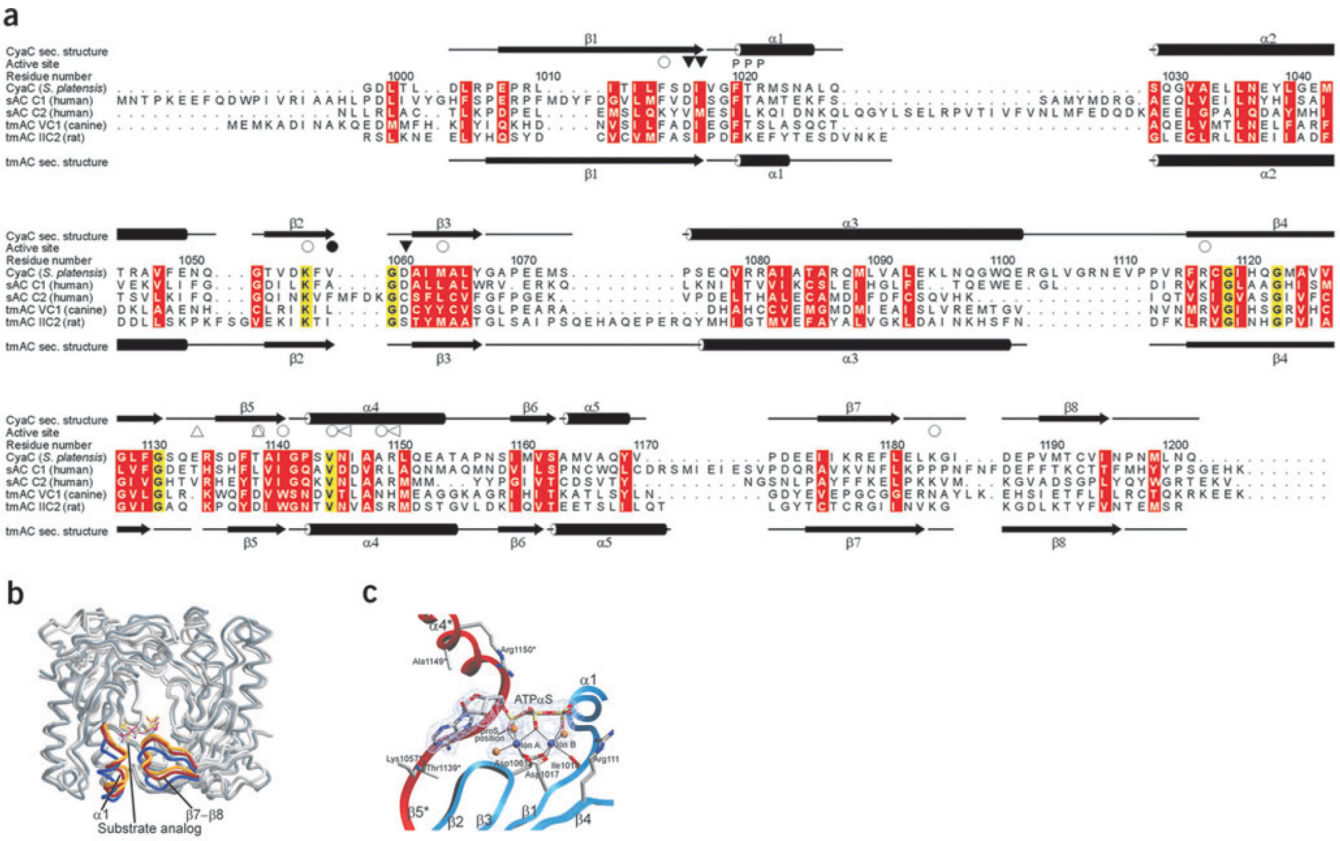

Figure 3.

Conformational states and comparison of AC enzymes. (**a**) Structure-based sequence alignment of bicarbonate responsive sAC enzymes and the G protein–regulated tmAC domains VC_1 and IIC_2 (PDB entry 1AZS). Secondary structure elements of sAC and IIC_2 are indicated on top and bottom, respectively. Ion-binding residues (▽) and residues binding the substrate (○) or the transition state (◁) are labeled (filled and empty symbols label C_1 and C_2 residues, respectively). Thr1139* and the insertion characteristic for sAC enzymes are indicated (△). Conserved amino acids are shaded yellow, and residues with conserved physicochemical properties are shaded red. (**b**) Overlay of the sAC–α,β-Me-ATP structure (open state, darkest gray, with α1 helix and β7–β8 loop in blue), the sAC–Rp-ATPαS complex (partially closed, middle gray and red), and the bicarbonate-soaked Rp-ATPαS structure (closed, lightest gray and yellow). Structures were superimposed on sAC–α,β-Me-ATP by optimizing positional agreement for residues 1014–1018, 1056–1065, 1117–1126 and 1143–1167 in both subunits. (**c**) sAC active site in complex with Rp-ATPαS and two magnesium ions, with the two monomers colored red and blue, respectively. The dashed lines indicate the octahedral coordination of the ions through the ATP analog, protein residues and one and two water molecules (gold spheres), respectively. The $2F_o - F_c$ omit electron density for the ligands was contoured at 1.1 σ. In its tmAC complex, Pα of Rp-ATPαS was modeled differently but with limited electron density for the ribose and its link to the Pα[16], and we speculate that this density might also be interpretable with the inhibitor conformation observed here for its sAC complex.

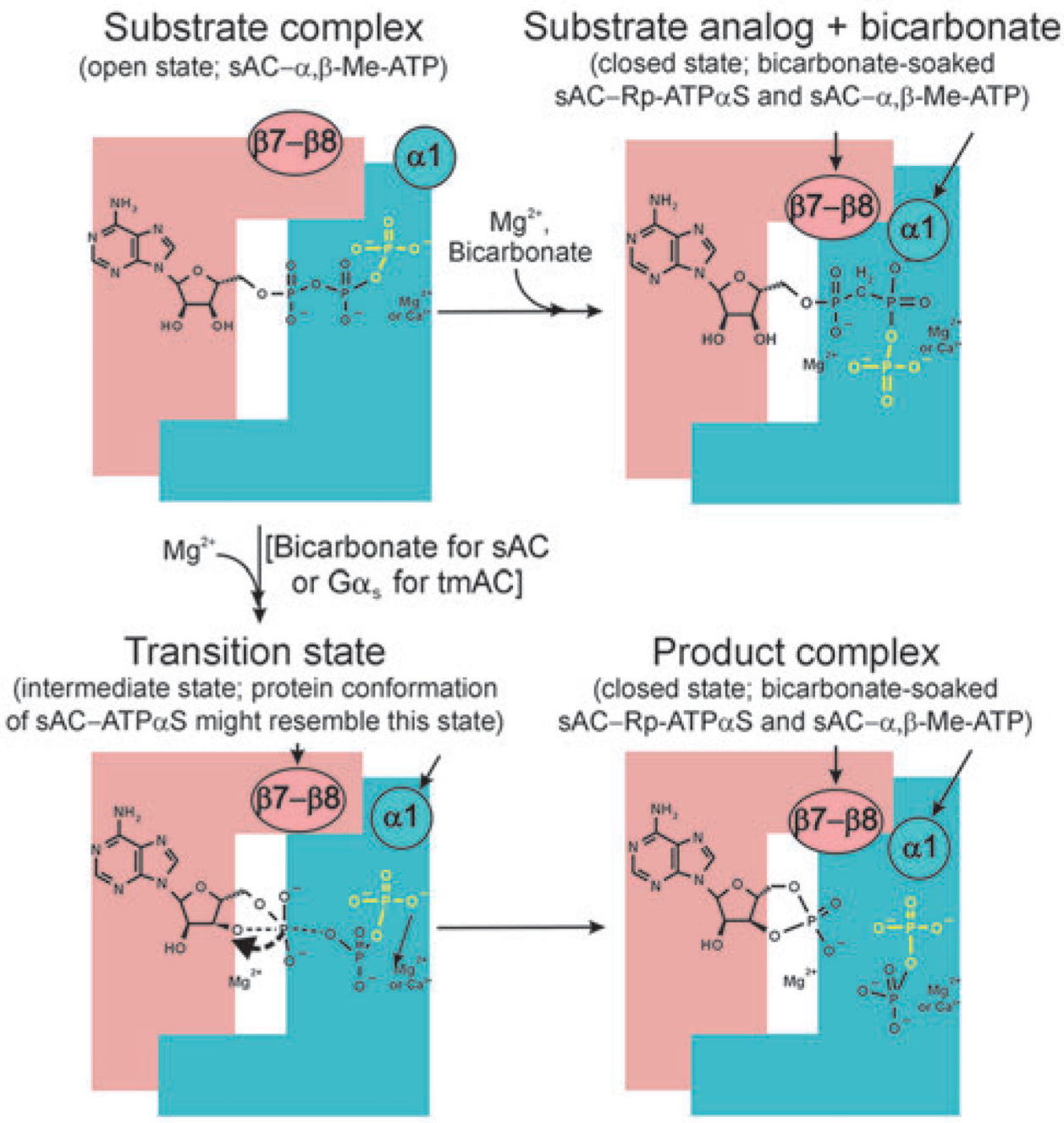

Figure 4.

Model for catalysis by class III nucleotidyl cyclases. The model for catalysis (bottom pathway) is based on the conformational changes observed with the sAC–substrate analog complexes (top). The arrows at α1 and β7–β8 indicate the movements undergone by these protein parts. The individual catalytic states (open, intermediate and closed) are extrapolated from the different sAC structures presented in the text, with the protein conformation of the sAC–Rp-ATPαS complex being a speculative approximate intermediate state.

Table 1

Data collection and refinement statistics

	CyaC Rp-ATPαS	CyaC α,β-Me-ATP	CyaC α,β-Me-ATP + $SrCl_2$	CyaC α,β-Me-ATP + $EuCl_3$	CyaC α,β-Me-ATP + bicarbonate	CyaC Rp-ATPαS + bicarbonate
Data collection						
Space group	$C222_1$	$P2_12_12_1$	$P2_12_12_1$	$P2_12_12_1$	$P2_1$	$C222_1$
Unit cell dimensions (Å)						
a	54.2	53.7	53.5	53.6	53.3	51.1
b	78.9	71.5	70.5	70.2	71.2	74.0
c	283.6	99.6	99.4	99.6	106.7	266.7
β(°)	90.0	90.0	90.0	90.0	95.8	90.0
Resolution (Å)	20.0–1.9	20.0–2.4	20.0–1.9	20.0–3.0	20.0–2.3	20.0–2.5
Unique reflections	48,991	15,574	30,126	8,038	33,968	14,233
$<I/\sigma>$	9.7	7.0	10.8	5.1	8.9	8.3
Completeness (%)[a]	99.6 (98.6)	99.2 (99.8)	98.8 (94.1)	99.4 (99.2)	95.0 (98.0)	80.0 (69.0)
R_{merge} (%)[a]	7.2 (36.7)	8.1 (34.4)	5.6 (21.7)	13.8 (36.2)	7.0 (42.2)	9.2 (27.7)
Refinement						
Resolution (Å)	15.0–1.93	15.0– 2.4	15.0–1.9	15.0–3.0	15.0–2.3	15.0–2.5
Total reflections used	40,595	12,704	25,021	5,601	26,793	11,732
No. atoms						
Protein	4,495	3,042	3,025	3,041	4,510	4,447
Ligand	99	64	64	64	132	99
Solvent	385	141	227	2	99	86
R.m.s. deviations						
Bond lengths (Å)	0.006	0.007	0.006	0.012	0.007	0.010
Bond angles (°)	1.2	1.4	1.2	1.6	1.2	1.5
Average *B*-factor (Å^2)	30.8	33.9	28.8	—	39.0	29.2
Final R_{cryst} / R_{free}(%)[b]	19.8 / 22.9	21.9 / 27.1	20.4 / 23.6	27.4 / 31.5	20.2/ 26.2	24.1 / 29.1

[a] Values in parentheses are for the highest-resolution shell.

[b] R_{free} was calculated from 6–7% of measured reflections omitted from refinement.